PERGAMON

International Journal of Solids and Structures 36 (1999) 5101–5123

INTERNATIONAL JOURNAL OF SOLIDS and STRUCTURES

www.elsevier.com/locate/ijsolstr

Differential quadrature element method for static analysis of Reissner–Mindlin polar plates

F.-L. Liu[a,*], K. M. Liew[b]

[a] *CAD/CAM Laboratory, School of Mechanical and Production Engineering, Nanyang Technological University, Singapore 639798*

[b] *Centre for Advanced Numerical Engineering Simulations, School of Mechanical and Production Engineering, Nanyang Technological University, Singapore 639798*

Received 8 April 1998

Abstract

In this paper, a new numerical technique, the differential quadrature element method (DQEM), has been developed for static analysis of the two-dimensional polar Reissner–Mindlin plate in the polar coordinate system by integrating the domain decomposition method (DDM) with the differential quadrature method (DQM). The detailed formulations for the sectorial DQEM plate bending element and the compatibility conditions between each element are presented. The convergence properties and the accuracy of the DQEM for bending of thick polar plates are investigated through a number of numerical computations. Consequently, the DQEM has been successfully applied to analyze several annular sector plates with discontinuous loading and boundary conditions and cutouts to illustrate the simplicity and flexibility of this method for solving Reissner–Mindlin plates in polar coordinate system which are not solvable directly using the differential quadrature method. The numerical results are verified by the existing exact solutions or the FEM solutions obtained using the software package ANSYS (Version 5.3).

1. Introduction

The differential quadrature method (DQM) is a numerical technique for solving initial and boundary value problems. It was originated by Bellman and his associates (Bellman and Casti, 1971; Bellman et al., 1972) and further extended to multi-dimensional problems by Civan and Sliepcevich (1984). It was first applied to structural analysis fields by Bert and his associates (Bert et al., 1988, 1989; Striz et al., 1988). Since then, many researches have been done in both the theoretical development and the engineering applications of the method. An excellent review paper

* Corresponding author

0020-7683/99/$ - see front matter
PII: S0020-7683(98)00245-5

contributed by Bert and Malik (1996a) has summarized a detailed literature list on both aspects of the DQM. It has been claimed by many researchers that this numerical method has the capability of yielding accurate solutions with minimal computational effort and therefore, has the potential to become an alternative to the conventional numerical methods (Bert et al., 1988, 1989; Pandya and Sherbourne, 1991; Bert and Malik, 1995; Liew et al., 1996; Bert and Malik, 1996a, b, c; Striz et al., 1994; Chen et al., 1997a, b). Nevertheless, the further application of the DQM has been greatly restricted by the disadvantage that it cannot be directly employed to solve the problem with discontinuities. To overcome such drawbacks, the quadrature element method (QEM) was developed to perform the static analysis of truss and beam and the free vibration analysis of thin plates (Striz et al., 1994; Chen et al., 1997a). However, for all the problems analyzed in Striz et al. (1994), a δ-grid arrangement was introduced, which uses two points, separated by a small distance δ, to present each boundary point in order to satisfy the multi-boundary conditions at one point. This is inconvenient and inaccurate for the differential equations of four or higher-order. An improvement on the δ-grid arrangement has been reported in their recent papers (Chen et al., 1997a, b) by incorporating the boundary conditions into the weighting coefficient matrices. However, the mathematical manipulations for the transformation of the weighting coefficient matrices and the governing equation matrix are very complicated and cumbersome for the higher-order governing equations (e.g., for sixth-order equations of thick Reissner–Mindlin plates, Reissner, 1945; Mindlin, 1951). Furthermore, since the QEM which was implemented for the plate problems by Chen et al. (1997a, b) was based on the classical thin plate theory, the effects of the transverse deformation and rotary inertia (for dynamic cases) were neglected. This results in a significant discrepancy between the computational results and the realistic values for thick plates. Han and Liew (1996) developed the one-dimensional differential quadrature element method (DQEM), for bending analysis of the axisymmetric circular Reissner–Mindlin plate. The present authors have developed the two-dimensional DQEM for static analysis of Reissner–Mindlin plate problems in a Cartesian coordinate system (Liu and Liew, 1998). It has been shown that the DQEM integrates the attractive advantages of both the high accuracy of the DQM and the great flexibility of the FEM for thick plate analysis of the rectangular and the one-dimensional axisymmetric circular plates (Han and Liew, 1996; Liu and Liew, 1998). In this paper, the two-dimensional DQEM has been further developed for bending analysis of two-dimensional Reissner–Mindlin polar plates in the polar coordinate system.

2. Formulations

Consider an annular sectorial Mindlin–Reissner plate with outer radius a, inner radius b and sector angle α. The plate is divided into N_E elements based on the discontinuities in the geometry, boundary constraints and materials used. Each element consists of an isotropic material and has uniform thickness and continuous boundary constrains on each edge.

2.1. Governing equations and constraint conditions

The equilibrium governing equations for a given element l of the sectorial Reissner–Mindlin plate in polar coordinates are given by Kobayashi and Sonoda (1987) as follows:

$$\frac{D_l}{2}\left\{(1-v_l)\left[\nabla^2\psi_r-\frac{1}{r^2}\psi_r-\frac{2}{r^2}\frac{\partial\psi_\theta}{\partial\theta}\right]+(1+v_l)\frac{\partial\phi}{\partial r}\right\}-\kappa G_l h_l\left(\psi_r+\frac{\partial w}{\partial r}\right)=0 \tag{1a}$$

$$\frac{D_l}{2}\left\{(1-v_l)\left[\nabla^2\psi_\theta-\frac{1}{r^2}\psi_\theta+\frac{2}{r^2}\frac{\partial\psi_r}{\partial\theta}\right]+(1+v_l)\frac{1}{r}\frac{\partial\phi}{\partial\theta}\right\}-\kappa G_l h_l\left(\psi_\theta+\frac{1}{r}\frac{\partial w}{\partial\theta}\right)=0 \tag{1b}$$

$$-\kappa G_l h_l(\nabla^2 w+\phi)-q_l=0 \tag{1c}$$

in which

$$\nabla^2=\frac{\partial^2}{\partial r^2}+\frac{1}{r}\frac{\partial}{\partial r}+\frac{1}{r^2}\frac{\partial^2}{\partial\theta^2} \tag{2a}$$

$$\phi=\frac{\partial\psi_r}{\partial r}+\frac{1}{r}\frac{\partial\psi_\theta}{\partial\theta}+\frac{1}{r}\psi_r \tag{2b}$$

where w is the transverse deflection; ψ_r and ψ_θ are the angular rotations of the normal to the mid-surface in radial and circumferential directions; h_l, E_l, G_l and v_l are the plate thickness, Young's modulus, shear modulus and Poisson's ratio, respectively; D_l is the plate flexural rigidity; and κ is the shear correction factor which is taken to be 5/6 (Reissner, 1947; Mindlin, 1951).

Substituting eqn (2) into eqn (1) yields

$$r^2\frac{\partial^2\psi_r}{\partial r^2}+r\frac{\partial\psi_r}{\partial r}-(1+\xi_l r^2)\psi_r+\frac{(1-v_l)}{2}\frac{\partial^2\psi_r}{\partial\theta^2}+\frac{(1+v_l)}{2}r\frac{\partial^2\psi_\theta}{\partial r\,\partial\theta}-\frac{(3-v_l)}{2}\frac{\partial\psi_\theta}{\partial\theta}-\xi_l r^2\frac{\partial w}{\partial r}=0 \tag{3a}$$

$$\frac{(1+v_l)}{2}r\frac{\partial^2\psi_r}{\partial r\,\partial\theta}+\frac{(3-v_l)}{2}\frac{\partial\psi_r}{\partial\theta}+\frac{\partial^2\psi_\theta}{\partial\theta^2}+\frac{(1-v_l)}{2}r^2\frac{\partial^2\psi_\theta}{\partial r^2}+\frac{(1-v_l)}{2}r\frac{\partial\psi_\theta}{\partial r}-\left[\frac{(1-v_l)}{2}+\xi_l r^2\right]\psi_\theta-\xi_l r\frac{\partial w}{\partial\theta}=0 \tag{3b}$$

$$\left(r^2\frac{\partial^2 w}{\partial r^2}+r\frac{\partial w}{\partial r}+\frac{\partial^2 w}{\partial\theta^2}\right)+\left(r^2\frac{\partial\psi_r}{\partial r}+r\psi_r\right)+r\frac{\partial\psi_\theta}{\partial\theta}=-\frac{r^2 q_l}{\kappa G_l h_l} \tag{3c}$$

in which

$$\xi_l=\frac{6\kappa(1-v_l^2)}{h_l^2} \tag{4}$$

The moment resultants M_r, M_θ and $M_{r\theta}$ and the shear force resultants Q_r and Q_θ can be written as

$$M_r=D_l\left(\frac{\partial\psi_r}{\partial r}+v_l\frac{1}{r}\left(\psi_r+\frac{\partial\psi_\theta}{\partial\theta}\right)\right) \tag{5a}$$

$$M_\theta = D_l\left(\frac{1}{r}\left(\psi_r + \frac{\partial \psi_\theta}{\partial \theta}\right) + v_l \frac{\partial \psi_r}{\partial r}\right) \tag{5b}$$

$$M_{r\theta} = \frac{1-v_l}{2} D_l\left(\frac{1}{r}\left(\frac{\partial \psi_r}{\partial \theta} - \psi_\theta\right) + \frac{\partial \psi_\theta}{\partial r}\right) \tag{5c}$$

$$Q_r = \kappa G_l h_l\left(\psi_r + \frac{\partial w}{\partial r}\right) \tag{5d}$$

$$Q_\theta = \kappa G_l h_l\left(\psi_\theta + \frac{1}{r}\frac{\partial w}{\partial \theta}\right) \tag{5e}$$

The boundary conditions for the radial and circumferential edges of the plate are expressed in polar coordinates as follows:

• Generalized hard simply supported edge (S):

$$w = 0, \quad \psi_\theta = 0, \quad M_r = (M_r^{\text{ext}})_1, \quad \text{at } r = b \tag{6a}$$

$$w = 0, \quad \psi_\theta = 0, \quad M_r = (M_r^{\text{ext}})_{I_E+1}, \quad \text{at } r = a \tag{6b}$$

$$w = 0, \quad \psi_r = 0, \quad M_\theta = (M_\theta^{\text{ext}})_1, \quad \text{at } \theta = 0 \tag{6c}$$

$$w = 0, \quad \psi_r = 0, \quad M_\theta = (M_\theta^{\text{ext}})_{J_E+1}, \quad \text{at } \theta = \alpha \tag{6d}$$

• Generalized soft simply supported edge (S′):

$$w = 0, \quad M_{r\theta} = 0, \quad M_r = (M_r^{\text{ext}})_1, \quad \text{at } r = b \tag{7a}$$

$$w = 0, \quad M_{r\theta} = 0, \quad M_r = (M_r^{\text{ext}})_{I_E+1}, \quad \text{at } r = a \tag{7b}$$

$$w = 0, \quad M_{r\theta} = 0, \quad M_\theta = (M_\theta^{\text{ext}})_1, \quad \text{at } \theta = 0 \tag{7c}$$

$$w = 0, \quad M_{r\theta} = 0, \quad M_\theta = (M_\theta^{\text{ext}})_{J_E+1}, \quad \text{at } \theta = \alpha \tag{7d}$$

• Clamped edge (C):

$$w = 0, \quad \psi_r = 0, \quad \psi_\theta = 0; \quad \text{at } r = b, a \quad \text{and} \quad \theta = 0, \alpha \tag{8a–c}$$

• Generalized free edge (F):

$$Q_r = (Q_r^{\text{ext}})_1, \quad M_r = (M_r^{\text{ext}})_1, \quad M_{r\theta} = 0 \quad \text{at } r = b \tag{9a}$$

$$Q_r = (Q_r^{\text{ext}})_{I_E+1}, \quad M_r = (M_r^{\text{ext}})_{I_E+1}, \quad M_{r\theta} = 0 \quad \text{at } r = a \tag{9b}$$

$$Q_\theta = (Q_\theta^{\text{ext}})_1, \quad M_\theta = (M_\theta^{\text{ext}})_1, \quad M_{r\theta} = 0 \quad \text{at } \theta = 0 \tag{9c}$$

$$Q_\theta = (Q_\theta^{\text{ext}})_{J_E+1}, \quad M_\theta = (M_\theta^{\text{ext}})_{J_E+1}, \quad M_{r\theta} = 0 \quad \text{at } \theta = \alpha \tag{9d}$$

where $(M_r^{\text{ext}})_1$, $(M_\theta^{\text{ext}})_1$, $(Q_r^{\text{ext}})_1$ and $(Q_\theta^{\text{ext}})_1$ are the external concentrated line moments and line

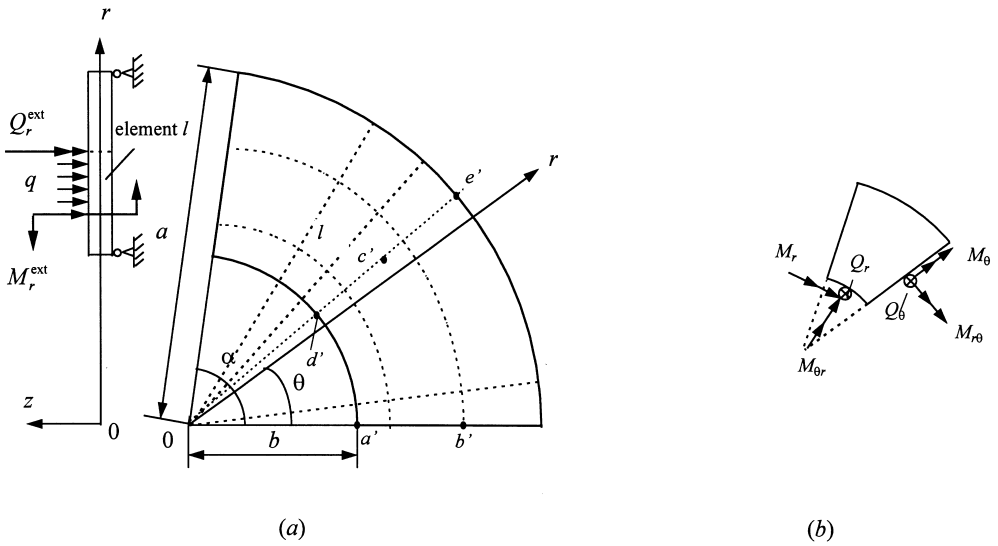

Fig. 1. Coordinate system and discretization of an annular sector plate with inner and outer radii b and a and sector angle α: (a) coordinate system; (b) positive directions of resultant moments and shear forces in plate.

loads at the sides $r = b$ and $\theta = 0$; and $(M_r^{ext})_{I_E+1}$, $(M_\theta^{ext})_{J_E+1}$, $(Q_r^{ext})_{I_E+1}$ and $(Q_\theta^{ext})_{J_E+1}$ are the external concentrated line moments and line loads at the sides $r = a$ and $\theta = \alpha$.

2.2. Sectorial DQEM plate bending element

The lth element is further divided into $N_r \times N_\theta$ grid points along the radial and circumferential directions, respectively. The element is subject to the 'external' concentrated line forces and moments, which are the combination action of the real external forces and moments applied at the four edges of element l and the shear forces and moments yielded by the adjacent elements as shown in Fig. 2. Using the DQM rule (Liew et al., 1996), the governing eqns (3a–c) can be discretized for each node on the inner grid of the element l as

$$\left[\sum_{k=1}^{N_y}(C_{ik}^{(2)}r_i^2+C_{ik}^{(1)}r_i)(\psi_r)_{kj}\right]-(1+\xi_l r_i^2)(\psi_r)_{ij}+\frac{1+\nu_l}{2}\left[\sum_{m=1}^{N_\theta}\bar{C}_{jm}^{(2)}(\psi_r)_{im}\right]$$
$$+\frac{1+\nu_l}{2}r_i\left[\sum_{k=1}^{N_r}C_{ik}^{(1)}\sum_{m=1}^{N_\theta}\bar{C}_{jm}^{(1)}(\psi_\theta)_{km}\right]-\frac{(3-\nu_l)}{2}\left[\sum_{m=1}^{N_\theta}\bar{C}_{jm}^{(1)}(\psi_\theta)_{im}\right]-\xi_l r_i^2\left[\sum_{k=1}^{N_r}C_{ik}^{(1)}(w)_{kj}\right]=0 \quad (10a)$$

$$\frac{1+\nu_l}{2}r_i\left[\sum_{k=1}^{N_r}C_{ik}^{(1)}\sum_{m=1}^{N_\theta}\bar{C}_{jm}^{(1)}(\psi_\theta)_{km}\right]+\frac{3-\nu_l}{2}\left[\sum_{m=1}^{N_\theta}\bar{C}_{jm}^{(1)}(\psi_r)_{im}\right]+\left[\sum_{m=1}^{N_\theta}\bar{C}_{jm}^{(2)}(\psi_\theta)_{im}\right]$$
$$+\frac{1-\nu_l}{2}\left[\sum_{k=1}^{N_r}(C_{ik}^{(2)}r_i^2+C_{ik}^{(1)}r_i)(\psi_\theta)_{kj}\right]-\left(\frac{1-\nu_l}{2}+\xi_l r_i^2\right)(\psi_\theta)_{ij}-\xi_l r_i\left[\sum_{m=1}^{N_\theta}\bar{C}_{jm}^{(1)}(w)_{im}\right]=0 \quad (10b)$$

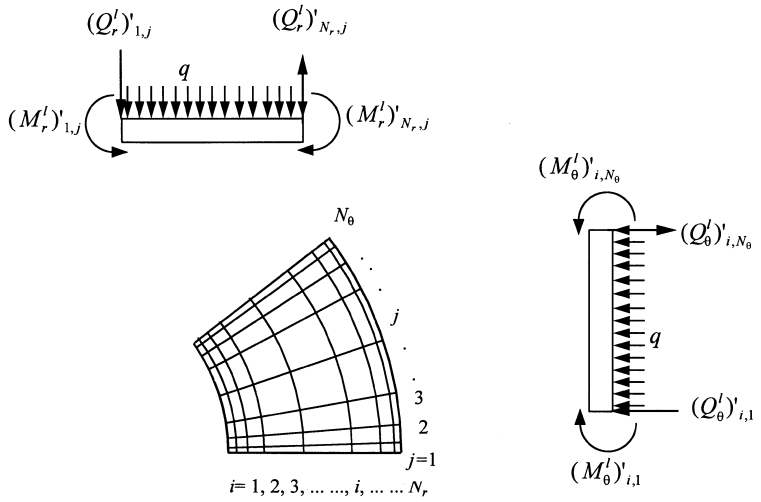

Fig. 2. Equilibrium and arrangement of grid points of element l.

$$\left[\sum_{k=1}^{N_r}(C_{ik}^{(2)}r_i^2+C_{ik}^{(1)}r_i)(w)_{kj}\right]+\left[\sum_{m=1}^{N_\theta}\bar{C}_{jm}^{(2)}(w)_{im}\right]+r_i^2\left[\sum_{k=1}^{N_r}C_{ik}^{(1)}(\psi_r)_{kj}\right]$$
$$+r_i(\psi_r)_{ij}+r_i\left[\sum_{m=1}^{N_\theta}\bar{C}_{jm}^{(1)}(\psi_\theta)_{im}\right]=-\frac{r_i^2q_l}{\kappa G_l h_l} \quad (10c)$$

where $i=1,2,\ldots,N_r; j=1,2,\ldots,N_\theta$; $C_{ik}^{(n)}$ and $\bar{C}_{r's}^{(n)}$ $(n=1,2; r'=1,2,3,\ldots,N_r; s=1,2,3,\ldots,N_\theta)$ are the weighting coefficients for the nth-order partial derivatives of w, ψ_r and ψ_θ with respect to r and θ, respectively.

Using the same procedures, the moments and shear forces expressed by eqns (5a–e) are discretized into

$$(M_r)_{ij}=D_l\left\{\sum_{k=1}^{N_r}C_{ik}^{(1)}(\psi_r)_{kj}+\nu_l\frac{1}{r_i}\left[(\psi_r)_{ij}+\sum_{m=1}^{N_\theta}\bar{C}_{jm}^{(1)}(\psi_\theta)_{im}\right]\right\} \quad (11a)$$

$$(M_\theta)_{ij}=D_l\left\{\frac{1}{r_i}\left[(\psi_r)_{ij}+\sum_{m=1}^{N_\theta}\bar{C}_{jm}^{(1)}(\psi_\theta)_{im}\right]+\nu_l\sum_{k=1}^{N_r}C_{ik}^{(1)}(\psi_r)_{kj}\right\} \quad (11b)$$

$$(M_{r\theta})_{ij}=\frac{(1-\nu_l)}{2}D_l\left\{\frac{1}{r_i}\left[\sum_{m=1}^{N_\theta}\bar{C}_{jm}^{(1)}(\psi_r)_{im}-(\psi_\theta)_{ij}\right]+\sum_{k=1}^{N_r}C_{ik}^{(1)}(\psi_\theta)_{kj}\right\} \quad (11c)$$

$$(Q_r)_{ij}=\kappa G_l h_l\left[(\psi_r)_{ij}+\sum_{k=1}^{N_r}C_{ik}^{(1)}(w)_{kj}\right] \quad (11d)$$

$$(Q_\theta)_{ij} = \kappa G_l h_l \left[(\psi_\theta)_{ij} + \frac{1}{r_i} \sum_{m=1}^{N_\theta} \bar{C}^{(1)}_{jm} (w)_{im} \right]$$

$$i = 2, 3, \ldots, N_r - 1; \quad j = 2, 3, \ldots, N_\theta - 1 \quad \text{and} \quad l = 1, 2, 3, \ldots, N_E \tag{11e}$$

For the grid points at the four edges of element l, the corresponding boundary conditions described by eqns (6)–(9) or the compatibility conditions should be applied. The details of the compatibility conditions for sectorial DQEM plate bending elements will be presented in Section 2.3.

In matrix form, eqns (10a–c) can be expressed as

$$\mathbf{K}^e \mathbf{d}^e = \mathbf{f}^e \tag{12}$$

in which $\mathbf{K}^e$, $\mathbf{d}^e$ and $\mathbf{f}^e$ are the element weighting coefficient matrix, element displacement vector and element force vector, respectively and

$$\begin{aligned}
\mathbf{d}^e = [&w_{1,1}, (\psi_r)_{1,1}, (\psi_\theta)_{1,1}, w_{1,2}, (\psi_r)_{1,2}, (\psi_\theta)_{1,2}, \ldots, w_{1,N_\theta}, (\psi_r)_{1,N_\theta}, \\
&(\psi_\theta)_{1,N_\theta}, w_{2,1}, (\psi_r)_{2,1}, (\psi_\theta)_{2,1}, w_{2,2}, (\psi_r)_{2,2}, (\psi_\theta)_{2,2}, \ldots, w_{2,N_\theta}, \\
&(\psi_r)_{2,N_\theta}, (\psi_\theta)_{2,N_\theta}, \ldots, w_{N_r,1}, (\psi_r)_{N_r,1}, (\psi_\theta)_{N_r,1}, w_{N_r,2}, \\
&(\psi_r)_{N_r,2}, (\psi_\theta)_{N_r 2}, \ldots, w_{N_r,N_\theta}, (\psi_r)_{N_r,N_\theta}, (\psi_\theta)_{N_r,N_\theta}]^T
\end{aligned} \tag{13}$$

$$\begin{aligned}
\mathbf{f}^e = [&(Q_r^l)'_{1,1}, (M_r^l)'_{1,1}, (M_{r\theta}^l)'_{1,1}, (Q_r^l)'_{1,2}, (M_r^l)'_{1,2}, (M_{r\theta}^l)'_{1,2}, \ldots, (Q_r^l)'_{1,N_\theta}, \\
&(M_r^l)'_{1,N_\theta}, (M_{r\theta}^l)'_{1,N_\theta}, (Q_\theta^l)'_{2,1}, (M_\theta^l)'_{2,1}, (M_{r\theta}^l)'_{2,1}, 0, 0, f_{2,2}, \\
&0, 0, f_{2,3}, \ldots, 0, 0, f_{2,N_\theta - 1}, (Q_\theta^l)'_{2,N_\theta}, (M_\theta^l)'_{2,N_\theta}, (M_{r\theta}^l)'_{2,N_\theta}, \ldots \\
&(Q_\theta^l)'_{N_r - 1,1}, (M_\theta^l)'_{N_r - 1,1}, (M_{r\theta}^l)'_{N_r - 1,1}, 0, 0, f_{N_r - 1,2}, 0, 0, f_{N_r - 1,3}, \ldots \\
&0, 0, f_{N_r - 1,N_r - 1}, (Q_\theta^l)'_{N_r - 1,N_\theta}, (M_\theta^l)'_{N_r - 1,N_\theta}, (M_{r\theta}^l)'_{N_r - 1,N_\theta}, (Q_r^l)'_{N_r,1}, \\
&(M_r^l)'_{N_r,1}, (M_{r\theta}^l)'_{N_r,1}, (Q_r^l)'_{N_r,2}, (M_r^l)'_{N_r,2}, (M_{r\theta}^l)'_{N_r,2}, \ldots \\
&(Q_r^l)'_{N_r,N_\theta}, (M_r^l)'_{N_r,N_\theta}, (M_{r\theta}^l)'_{N_r,N_\theta}]^T
\end{aligned} \tag{14}$$

2.3. Assembly of plate elements and compatibility conditions

In order to obtain a complete solution for the entire plate, a global system equation for all the nodal points of the plate labelled from 1 to N should be established. This can be done by assembling the weighting coefficient matrices, the displacement vector and the force vector of all the elements. The final global matrix forms of the equation system for the whole plate are

$$\mathbf{K}\mathbf{d} = \mathbf{F} \tag{15}$$

where $\mathbf{K}$, $\mathbf{d}$ and $\mathbf{F}$ represent the overall weighting coefficient matrix, global displacement vector and global force and moment vector for the entire plate, respectively and

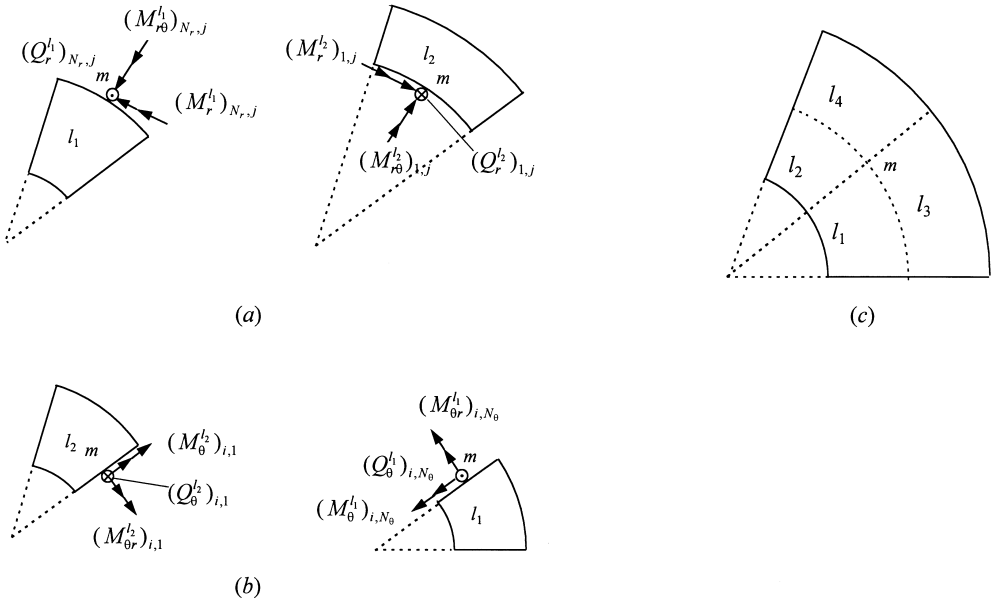

Fig. 3. Locations of the conjunction nodes on the interface boundaries of sectorial elements: (a) two sectorial elements are connected in r-direction; (b) two elements are connected in θ-direction; and (c) four sectorial elements are connected at point m.

$$\mathbf{d} = [w_1,(\psi_r)_1,(\psi_\theta)_1, w_2,(\psi_r)_2,(\psi_\theta)_2, \ldots, w_N,(\psi_r)_N,(\psi_\theta)_N]^T \tag{16}$$

The successful solution of the problem for the plate can be achieved only if the two conditions of (a) displacement compatibility and (b) equilibrium are satisfied at the interface boundaries of the plate. Obviously, the displacement compatibility conditions are automatically satisfied at all the interface conjunction nodes since the same global nodal number is used for each conjunction node. Only the equilibrium conditions are needed to form the compatibility conditions. Hence, according to the locations of the conjunction nodes, the compatibility conditions for the sectorial DQEM plate bending elements in polar coordinates are built up as follows:

• For conjunction nodes at which two elements meet

Suppose elements l_1 and l_2 are two adjacent sectorial elements in polar coordinates as shown in Fig. 3. In Fig. 3(a), the two elements are connected along the r-direction, while in Fig. 3(b), they are connected along the θ-direction. For the first case, the compatibility conditions for the conjunction nodes at the interface edge of elements l_1 and l_2 can be written according to the equilibrium condition as

$$(Q_r^{l_1})_{N_r,j} - (Q_r^{l_2})_{1,j} = (Q_r^{\text{ext}})_m \tag{17a}$$

$$(M_r^{l_1})_{N_r,j} - (M_r^{l_2})_{1,j} = (M_r^{\text{ext}})_m \tag{17b}$$

$$(M_{r\theta}^{l_1})_{N_r,j} - (M_{r\theta}^{l_2})_{1,j} = (M_{r\theta}^{\text{ext}})_m \tag{17c}$$

Similarly, the compatibility conditions for the conjunction nodes of elements l_1 and l_2 for the second case are

$$(Q_\theta^{l_1})_{i,N_\theta} - (Q_\theta^{l_2})_{i,1} = (Q_\theta^{\text{ext}})_m \tag{18a}$$

$$(M_\theta^{l_1})_{i,N_\theta} - (M_\theta^{l_2})_{i,1} = (M_\theta^{\text{ext}})_m \tag{18b}$$

$$(M_{r\theta}^{l_1})_{i,N_\theta} - (M_{r\theta}^{l_2})_{i,1} = (M_{r\theta}^{\text{ext}})_m \tag{18c}$$

• For conjunction nodes at which four elements meet

As shown in Fig. 3(c), four adjacent elements l_1, l_2, l_3 and l_4 are arbitrarily selected from the plate elements and all these four elements share one common node at their corners. Suppose the globally labeled number of the common conjunction node is m, then the compatibility conditions for the point m can be expressed as

$$(Q_r^{l_1})_{N_r,N_\theta} + (Q_r^{l_2})_{N_r,1} - (Q_r^{l_3})_{1,N_\theta} - (Q_r^{l_4})_{1,1} = (Q_r^{\text{ext}})_m \tag{19a}$$

$$(M_r^{l_1})_{N_r,N_\theta} + (M_r^{l_2})_{N_r,1} - (M_r^{l_3})_{1,N_\theta} - (M_r^{l_4})_{1,1} = (M_r^{\text{ext}})_m \tag{19b}$$

$$(M_{r\theta}^{l_1})_{N_r,N_\theta} + (M_{r\theta}^{l_2})_{N_r,1} - (M_{r\theta}^{l_3})_{1,N_\theta} - (M_{r\theta}^{l_4})_{1,1} = (M_{r\theta}^{\text{ext}})_m \tag{19c}$$

and

$$(Q_\theta^{l_1})_{N_r,N_\theta} - (Q_\theta^{l_2})_{N_r,1} + (Q_\theta^{l_3})_{1,N_\theta} - (Q_\theta^{l_4})_{1,1} = (Q_\theta^{\text{ext}})_m \tag{20a}$$

$$(M_\theta^{l_1})_{N_r,N_\theta} - (M_\theta^{l_2})_{N_r,1} + (M_\theta^{l_3})_{1,N_\theta} - (M_\theta^{l_4})_{1,1} = (M_\theta^{\text{ext}})_m \tag{20b}$$

$$(M_{r\theta}^{l_1})_{N_r,N_\theta} + (M_{r\theta}^{l_2})_{N_r,1} - (M_{r\theta}^{l_3})_{1,N_\theta} - (M_{r\theta}^{l_4})_{1,1} = (M_{r\theta}^{\text{ext}})_m \tag{20c}$$

• For conjunction nodes located at the boundaries of the plate

Take the inner side boundary ($r = b$) of the annular sectorial plate for example, by considering the compatibility conditions as well as the boundary conditions, the modified boundary conditions for the conjunction node m located at this boundary can be expressed as follows

$$w_m = 0, \quad \psi_{rm} = 0, \quad \psi_{\theta m} = 0 \quad \text{(for clamped side—remain unchanged)} \tag{21a–c}$$

$$w_m = 0, \quad \psi_{\theta m} = 0, \quad (M_r^{l_1})_{1,N_\theta} + (M_r^{l_2})_{1,1} = (M_r^{\text{ext}})_m \quad \text{(for hard simply supported side)} \tag{22a–c}$$

$$w_m = 0, \quad (M_r^{l_1})_{1,N_\theta} + (M_r^{l_2})_{1,1} = (M_r^{\text{ext}})_m, \quad (M_{r\theta}^{l_1})_{1,N_\theta} + (M_{r\theta}^{l_2})_{1,1} = (M_{r\theta}^{\text{ext}})_m$$

(for soft simply supported side) (23a–c)

$$(Q_r^{l_1})_{1,N_\theta} + (Q_r^{l_2})_{1,1} = (Q_r^{\text{ext}})_m, \quad (M_r^{l_1})_{1,N_\theta} + (M_r^{l_2})_{1,1} = (M_r^{\text{ext}})_m$$

$$(M_{r\theta}^{l_1})_{1,N_\theta} + (M_{r\theta}^{l_2})_{1,1} = (M_{r\theta}^{\text{ext}})_m \quad \text{(for free side)} \tag{24a–c}$$

3. Convergence and accuracy studies

Based on the aforementioned DQEM formulations, a program has been built up to solve the bending problems of the thick polar plates. The notation, for instance CSFS′, denotes an annular sector plate with edges $r = b$, $\theta = 0$, $r = a$ and $\theta = \alpha$ having clamped (C), hard simply supported (S), free (F) and soft simply supported (S′) boundary conditions, respectively. The cosine mesh pattern for each element has been employed for all the computations. It is expressed in the polar coordinates as follows:

$$r_i = b + \frac{(a-b)}{2}\{1-\cos[(i-1)\pi/(N_r-1)]\}; \quad i = 1, 2, 3, \ldots, N_r \tag{25a}$$

$$\theta_j = \frac{\alpha}{2}\{1-\cos[(j-1)\pi/(N_\theta-1)]\}; \quad j = 1, 2, 3, \ldots, N_\theta \tag{25b}$$

The convergence and accuracy studies are carried out first to examine the reliability of the DQEM for the bending solution of the Reissner–Mindlin plate in polar coordinates. The convergence rate is dependent upon the boundary conditions, relative thickness, sector angle and inner to outer radii ratio of the plate.

3.1. Influences of boundary conditions and relative thickness

To examine the effects of boundary conditions and relative thickness on the convergence rate and accuracy of the DQEM solutions for the polar plates, a uniformly loaded annular sector plate with three different boundary conditions, SSSS, CSCS and FSFS are studied. The convergence patterns for the thin ($h/l_c = 0.01$, where $l_c = a-b$) plates are shown in Figs 4–6. The relative

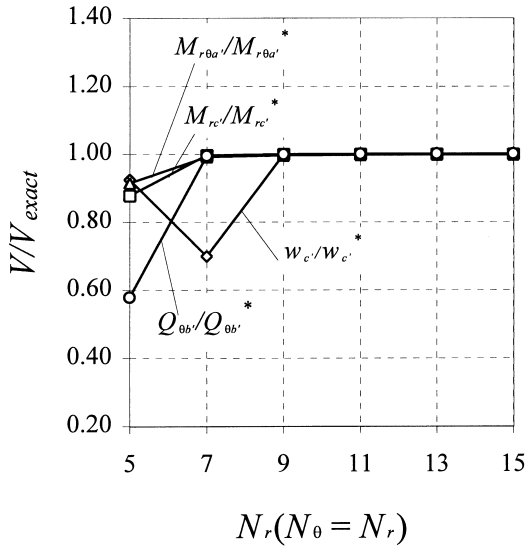

Fig. 4. Convergence patterns of the DQEM results for central deflection, moments and shear force of a thin SSSS annular sector plate ($h/l_c = 0.01, b/a = 0.5, \alpha = 30^\circ$).

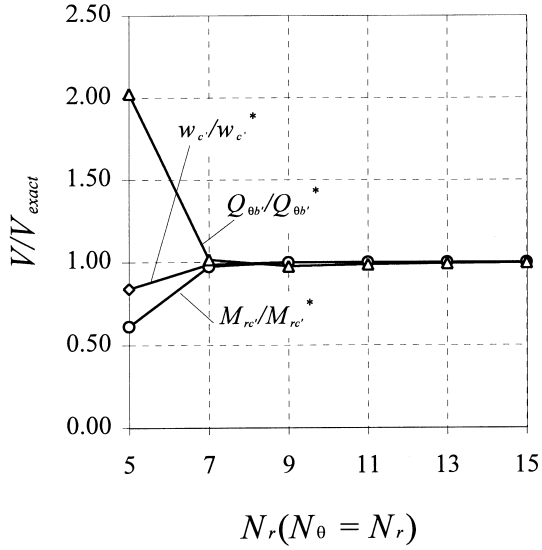

Fig. 5. Convergence patterns of the DQEM results for central deflection, moments and shear force of a thin CSCS annular sector plate ($h/l_c = 0.01, b/a = 0.5, \alpha = 30^\circ$).

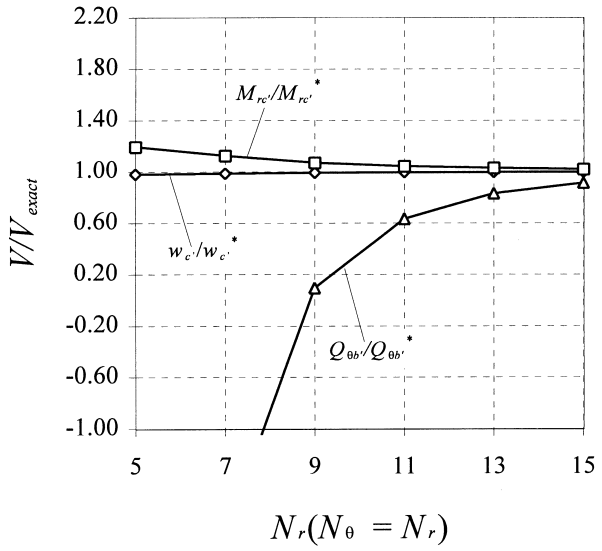

Fig. 6. Convergence patterns of the DQEM results for central deflection, moments and shear force of a thin FSFS annular sector plate ($h/l_c = 0.01, b/a = 0.5, \alpha = 30^\circ$).

percentage errors, defined as: error $= [(\text{Value})_{\text{DQEM}} - (\text{Value})_{\text{exact}}]/(\text{Value})_{\text{exact}} \times 100\%$, between the present DQEM results and the exact solution of Kobayashi and Turvey (1994) are presented in Tables 1–3. Furthermore, since it has been found by the present authors (Liu and Liew, 1998) that

Table 1
Convergence of numerical results of a uniformly loaded and simply supported annular sector plate with the increasing number of grid points in each element ($b/a = 0.5; \alpha = 30^\circ; \nu = 0.3; N_E = 2 \times 2$)[a]

h/l_c	$N_r \times N_\theta$	$W_{c'}$	Error (%)	$\bar{M}_{rc'}$	Error (%)	$\bar{M}_{\theta c'}$	Error (%)	$\bar{M}_{r\theta a'}$	Error (%)	$\bar{Q}_{rd'}$	Error (%)	$\bar{Q}_{rf'}$	Error (%)	$\bar{Q}_{\theta b'}$	Error (%)
0.01	5×5	2.16809	−7.44151	2.77205	−12.0849	3.64692	−10.8093	−2.70372	−8.39195	0.28301	−4.48532	−0.26862	−1.85605	0.17745	−42.1422
	7×7	2.33692	−0.23395	3.14479	−0.26355	4.08220	−0.16386	−2.92737	−0.81419	0.29569	−0.20587	−0.27115	−0.93168	0.30540	−0.42387
	9×9	2.34210	−0.01281	3.15276	−0.01078	4.08875	−0.00367	−2.94153	−0.33442	0.29624	−0.02025	−0.27323	−0.17172	0.30682	0.03913
	11×11	2.34240	0.00000	3.15316	0.00190	4.08903	0.00318	−2.94498	−0.21752	0.29646	0.05400	−0.27355	−0.05480	0.30707	0.12064
	13×13	2.34241	0.00043	3.15314	0.00127	4.08902	0.00294	−2.94686	−0.15383	0.29647	0.05737	−0.27364	−0.02192	0.30717	0.15324
	15×15	2.34241	0.00043	3.15313	0.00095	4.08900	0.00245	−2.94828	−0.10571	0.29642	0.04050	−0.27368	−0.00731	0.30722	0.16955
	Exact[b]	2.3424	—	3.1531	—	4.0889	—	−2.9514	—	0.2963	—	−0.2737	—	0.3067	—
0.20	5×5	2.94334	−1.12070	3.10987	−1.38980	4.03643	−1.32426	−2.96193	−1.87736	0.28532	−0.51604	−0.27777	0.97056	0.30763	0.27054
	7×7	2.97665	−0.00168	3.15372	0.00063	4.09074	0.00342	−3.01586	−0.09077	0.28706	0.09066	−0.27553	0.15631	0.30780	0.32595
	9×9	2.97674	0.00134	3.15372	0.00063	4.09068	0.00196	−3.01864	0.00133	0.28686	0.02092	−0.27532	0.07997	0.30755	0.24446
	11×11	2.97673	0.00101	3.15373	0.00095	4.09063	0.00073	−3.01869	0.00298	0.28684	0.01395	−0.27521	0.03999	0.30744	0.20861
	13×13	2.97673	0.00101	3.15372	0.00063	4.09062	0.00049	−3.01865	0.00166	0.28683	0.01046	−0.27517	0.02545	0.30740	0.19557
	15×15	2.97673	0.00101	3.15372	0.00063	4.09062	0.00049	−3.01862	0.00066	0.28682	0.00697	−0.27515	0.01818	0.30738	0.18905
	Exact[b]	2.9767	—	3.1537	—	4.0906	—	−3.0186	—	0.2868	—	−0.2751	—	0.3068	—

[a] $W_{c'} = w_{c'}/(10^{-3} \times q l_c^4/D)$; $\bar{M}_{rc'} = M_{rc'}/(10^{-2} \times q l_c^2)$; $\bar{M}_{\theta c'} = M_{\theta c'}/(10^{-2} \times q l_c^2)$; $\bar{M}_{r\theta a'} = M_{r\theta a'}/(10^{-2} \times q l_c^2)$; $\bar{Q}_{rd'} = Q_{rd'}/q l_c$; $\bar{Q}_{rf'} = Q_{rf'}/q l_c$; $\bar{Q}_{\theta b'} = Q_{\theta b'}/q l_{c'}$.
[b] Exact solution (Kobayashi and Turvey, 1994).

Table 2
Convergence of numerical results of a uniformly loaded annular sector plate having CSCS boundary conditions with the increasing number of grid points in each element ($b/a = 0.5; \alpha = 30^\circ; \nu = 0.3; N_E = 2\times 2$)[a]

h/l_c	$N_r \times N_\theta$	$W_{c'}$	Error (%)	$\bar{M}_{rc'}$	Error (%)	$\bar{M}_{\theta c'}$	Error (%)	$\bar{Q}_{rd'}$	Error (%)	$\bar{Q}_{re'}$	Error (%)	$\bar{Q}_{\theta b'}$	Error (%)
0.01	5×5	1.18221	−15.8689	1.60089	−38.5361	1.92557	−26.6058	0.57503	−5.18879	−0.38284	−9.17200	0.49369	102.001
	7×7	1.38673	−1.31440	2.53635	−2.62036	2.58429	−1.49832	0.60478	−0.28359	−0.41544	−7.31673	0.24753	1.28069
	9×9	1.40465	−0.03914	2.60329	−0.05030	2.62328	−0.01220	0.60400	−0.41220	−0.42129	−0.04982	0.23774	−2.72504
	11×11	1.40569	0.03487	2.60627	0.06412	2.32483	0.04688	0.60376	−0.45177	−0.42189	0.09253	0.24035	−1.65712
	13×13	1.40567	0.03345	2.60609	0.05721	2.62468	0.04117	0.60308	−0.56389	−0.42192	0.09964	0.24208	−0.94926
	15×15	1.40560	0.02847	2.60581	0.04646	2.62449	0.03392	0.60233	−0.68755	−0.42184	0.08066	0.24314	−0.51555
	Exact[b]	1.4052	—	2.6046	—	2.6236	—	0.6005	—	−0.4215	—	0.2444	—
0.20	5×5	2.17486	−1.71901	2.46519	−1.80528	2.99543	−1.80528	0.44175	2.18598	−0.39283	0.69982	0.25138	−1.95788
	7×7	2.21394	0.04700	2.55478	0.09966	3.05354	0.09966	0.43380	0.34698	−0.39066	0.14355	0.25681	0.15991
	9×9	2.21308	0.00813	2.55684	0.01180	3.05086	0.01180	0.43240	0.02313	−0.39031	0.05383	0.25706	0.25741
	11×11	2.21295	0.00226	2.55698	0.00098	3.05053	0.00098	0.43230	0.00000	−0.39019	0.02307	0.25699	0.23011
	13×13	2.21294	0.00181	2.55699	0.00000	3.05050	0.00000	0.43229	−0.00231	−0.39015	0.01282	0.25695	0.21451
	15×15	2.21294	0.00181	2.55698	0.00000	3.05050	0.00000	0.43229	−0.00231	−0.39013	0.00769	0.25693	0.20671
	Exact[b]	2.2129	—	2.5570	—	3.0505	—	0.4323	—	−0.3901	—	0.2564	—

[a] $W_{c'} = w_{c'}/(10^{-3}\times ql_c^4/D)$; $\bar{M}_{rc'} = M_{rc'}/(10^{-2}\times ql_c^2)$; $\bar{M}_{\theta c'} = M_{\theta c'}/(10^{-2}\times ql_c^2)$; $\bar{Q}_{rd'} = Q_{rd'}/ql_c$; $\bar{Q}_{re'} = Q_{re'}/ql_c$; $\bar{Q}_{\theta b'} = Q_{\theta b'}/ql_{c'}$.
[b] Exact solution (Kobayashi and Turvey, 1994).

Table 3
Convergence of numerical results of a uniformly loaded annular sector plate having FSFS boundary conditions with the increasing number of grid points in each element ($b/a = 0.5; \alpha = 30^\circ; \nu = 0.3; N_E = 2 \times 2$)[a]

h/l_c	$N_r \times N_\theta$	$W_{c'}$	Error (%)	$\bar{M}_{rc'}$	Error (%)	$\bar{M}_{\theta c'}$	Error (%)	$\bar{Q}_{\theta b'}$	Error (%)
0.01	5×5	5.91218	−2.10650	1.58080	19.7032	8.30180	0.15684	−5.18753	−1465.50
	7×7	5.94960	−1.48690	1.48783	12.6632	8.24520	−0.52601	−0.69079	−281.835
	9×9	5.98989	−0.81978	1.41392	7.06649	8.26223	−0.32055	0.03642	−90.4133
	11×11	6.00905	−0.50253	1.37898	4.42072	8.27223	−0.19991	0.24068	−36.6465
	13×13	6.01974	−0.32553	1.35915	2.91913	8.27809	−0.12921	0.31479	−17.1387
	15×15	6.02638	−0.21558	1.34655	1.96502	8.28176	−0.08493	0.34658	−8.77073
	17×17	6.03079	−0.14256	1.33800	1.31758	8.28419	−0.05562	0.36193	−4.73019
	Exact[b]	6.0394	—	1.3206	—	8.2888	—	0.3799	—
0.20	5×5	6.94667	−0.42044	1.11912	0.85511	8.33796	−0.07718	0.36591	−2.50200
	7×7	6.97216	−0.05505	1.11294	0.28293	8.34246	−0.02325	0.37513	−0.04530
	9×9	6.97580	−0.00287	1.11008	0.02523	8.34424	−0.00192	0.37576	0.12257
	11×11	6.97603	0.00043	1.10985	0.00451	8.34436	−0.00048	0.37580	0.13323
	13×13	6.97604	0.00057	1.10984	0.00360	8.34436	−0.00048	0.37580	0.13323
	15×15	6.97604	0.00057	1.10984	0.00360	8.34436	−0.00048	0.37580	0.13323
	17×17	6.97604	0.00057	1.10984	0.00360	8.34436	−0.00048	0.37580	0.13323
	Exact[b]	6.9760	—	1.1098	—	8.3444	—	0.3753	—

[a] $W_{c'} = w_{c'}/(10^{-3} \times q l_c^4/D)$; $\bar{M}_{rc'} = M_{rc'}/(10^{-2} \times q l_c^2)$; $\bar{M}_{\theta c'} = M_{\theta c'}/(10^{-2} \times q l_c^2)$; $\bar{Q}_{\theta b'} = Q_{\theta b'}/q l_c$.
[b] Exact solution (Kobayashi and Turvey, 1994).

the convergence rate of the DQEM is much more dominated by the grid points in each element than by the number of the discretized elements, the effect of the grid points in each element with a fixed number of elements is investigated here. For generality, the number of the discretized elements is fixed at 2×2. It is observed that no matter what boundary conditions are considered, all the results of the normalized deflection, moments and shear forces at the given points of the annular sector plate, as shown in Fig. 1, converge to the corresponding exact solutions with the increasing number of grid points in each element. It is also observed that as the grid points in each element increase, the normalized deflection and bending moments converge rapidly, while the transverse shear forces converge relatively slowly. Especially for the transverse shear force at the middle of the radial edge of the FSFS sector plate with the relative thickness ratio $h/l_c = 0.01$, 15×15 grid points used in each element still lead to a relative error of 8.7707%. Therefore, more grid points may be needed to furnish the converged shear forces at this point. By examining the three Tables, it is evident that as the relative thickness h/l_c increases from 0.01–0.2, the convergence rate has been improved. For example, in the case of the FSFS sector plate with $b/a = 0.5$ and $\alpha = 30^\circ$, when the h/l_c ratio is 0.2, 9×9 grid points in each element are able to produce the converged results for $W_{c'}$, $\bar{M}_{rc'}$ and $\bar{M}_{\theta c'}$ with the relative errors all less than 0.03%. When the h/l_c ratio is 0.01, 9×9 grid points used in each element lead to a relative error or less than 1% for $W_{c'}$, and $\bar{M}_{\theta c'}$. But for $\bar{M}_{rc'}$ and $\bar{Q}_{\theta b'}$, even though the grid points used in each element are as high as 17×17, the corresponding relative errors are still 1.3176 and 4.73019%, respectively. However, all these errors

Table 4
Effect of sector angle, α, on convergence and accuracy of numerical results of a uniformly loaded annular sector plate having CSCS boundary conditions with the increasing number of grid points in each element ($b/a = 0.5; h/l_c = 0.01; v = 0.3; N_E = 2 \times 2$)[a]

α	$N_r \times N_\theta$	$W_{c'}$	Error (%)	$\bar{M}_{rc'}$	Error (%)	$\bar{M}_{\theta c'}$	Error (%)	$\bar{Q}_{\theta b'}$	Error (%)
30°	5 × 5	1.18221	−15.8690	1.60089	−38.5360	1.92557	−26.6060	0.49369	102.001
	7 × 7	1.38673	−1.31440	2.53635	−2.62040	2.58429	−1.49830	0.24753	1.28070
	9 × 9	1.40465	−0.03910	2.60329	−0.05030	2.62328	−0.01220	0.23774	−2.72500
	11 × 11	1.40569	0.03490	2.60627	0.06410	2.62483	0.04690	0.24035	−1.65710
	13 × 13	1.40567	0.03340	2.60609	0.05720	2.62468	0.04120	0.24208	−0.94930
	15 × 15	1.40560	0.02850	2.60581	0.04650	2.62449	0.03390	0.24314	−0.51550
	Exact[b]	1.4052	—	2.6046	—	2.6236	—	0.2444	—
60°	5 × 5	2.21961	−12.1329	3.19503	−21.8303	1.01271	−42.1408	0.61927	159.870
	7 × 7	2.50440	−0.85903	4.04342	−1.07365	1.71618	−1.94938	0.23786	−0.18464
	9 × 9	2.52647	0.01465	4.08966	0.05774	1.75315	0.16283	0.23073	−3.17667
	11 × 11	2.52652	0.01663	4.08812	0.02006	1.75058	0.01600	0.23417	−1.73311
	13 × 13	2.52643	0.013106	4.08790	0.01468	1.75039	0.00514	0.23619	−0.88544
	15 × 15	2.52637	0.010769	4.08779	0.01199	1.75037	0.00400	0.23739	−0.38187
	Exact[b]	2.5261	—	4.0873	—	1.7503	—	0.2383	—
90°	5 × 5	2.35713	—	3.42799	—	0.58520	—	0.61704	—
	7 × 7	2.61072	—	4.09630	—	1.21539	—	0.23582	—
	9 × 9	2.64244	—	4.17752	—	1.34737	—	0.22840	—
	11 × 11	2.64326	—	4.17675	—	1.34566	—	0.23316	—
	13 × 13	2.64306	—	4.17585	—	1.34445	—	0.23543	—
	15 × 15	2.64301	—	4.17579	—	1.34441	—	0.23665	—

[a] $W_{c'} = w_{c'}/(10^{-3} \times q l_c^4/D)$; $\bar{M}_{rc'} = M_{rc'}/(10^{-2} \times q l_c^2)$; $\bar{M}_{\theta c'} = M_{\theta c'}/(10^{-2} \times q l_c^2)$; $\bar{Q}_{\theta b'} = Q_{\theta b'}/q l_c$.
[b] Exact solution (Kobayshi and Turvey, 1994).

are below the allowable precision limits for engineering applications. Further comparing the data between each of the three Tables, it is found that the convergence rates of the normalized deflection, moments and shear forces are also influenced by the boundary conditions of the plate. Generally, the SSSS sector plate has the faster convergence rate than the CSCS sector plate and the CSCS sector plate has the faster convergence rate than the FSFS sector plate.

3.2. Influences of sector angle and inner to outer radii ratio

In order to investigate the effects of the sector angle α and the inner to outer radii ratio, b/a, on the convergence and accuracy of the DQEM results, the uniformly loaded annular sector plate with CSCS boundary conditions is analyzed again. The relative thickness of the plate is taken to be 0.01. The numerical results obtained using the DQEM are shown in Tables 4 and 5. In Table 4, the effects of the sector angle α on the convergence rate and accuracy are investigated. It is found that the convergence rate increases as the sector angle α increases from 30–60° but decreases slightly when the sector angle increases from 60–90°. However, the overall effect of the sector angle is not significant.

Table 5
Effect of inner to outer radii ratio, b/a, on convergence of numerical results of a uniformly loaded annual sector plate having CSCS boundary conditions with the increasing number of grid points in each element ($\alpha = 60^\circ; h/l_c = 0.01; \nu = 0.3; N_E = 2\times 2$)[a]

b/a	$N_r \times N_\theta$	$W_{c'}$	Error (%)	$\bar{M}_{rc'}$	Error (%)	$\bar{M}_{\theta c'}$	Error (%)	$\bar{Q}_{\theta b'}$	Error (%)
0.10	5×5	0.76916	−16.1761	1.22067	−39.2075	1.71723	−26.6342	0.84040	263.699
	7×7	0.83996	−8.46021	1.56385	−22.1163	2.05706	−12.1155	0.39902	72.6836
	9×9	0.88152	−3.93095	1.81887	−9.41567	2.21060	−5.55575	0.26281	13.7361
	11×11	0.90494	−1.37861	1.94435	−3.16645	2.29565	−1.92212	0.23388	1.21608
	13×13	0.91452	−0.33457	1.99292	−0.74754	2.32984	−0.46141	0.23028	−0.34189
	15×15	0.91759	0.00000	2.00793	0.00000	2.34064	0.00000	0.23107	0.00000
0.25	5×5	1.31533	−19.1487	1.66854	−43.9178	1.69038	−34.0368	1.25564	414.480
	7×7	1.54941	−4.76012	2.66894	−10.2929	2.39220	−6.64986	0.34246	40.3180
	9×9	1.61370	−0.80831	2.92792	−1.58814	2.53542	−1.06103	0.24490	0.34418
	11×11	1.62542	−0.08790	2.97055	−0.15529	2.55998	−0.10263	0.24066	−1.39310
	13×13	1.62687	0.00123	2.97534	0.00571	2.56274	0.00507	0.24255	−0.61870
	15×15	1.62685	0.00000	2.97517	0.00000	2.56261	0.00000	0.24406	0.00000
0.50	5×5	2.21961	−12.1329	3.19503	−21.8303	1.01271	−42.1408	0.61927	159.870
	7×7	2.50440	−0.85903	4.04342	−1.07357	1.71618	−1.94938	0.23786	−0.18464
	9×9	2.52647	0.01465	4.08966	0.05774	1.75315	0.16283	0.23073	−3.17667
	11×11	2.52652	0.01663	4.08812	0.02006	1.75058	0.01600	0.23417	−1.73311
	13×13	2.52643	0.01306	4.08790	0.01468	1.75039	0.00514	0.23619	−0.88544
	15×15	2.52637	0.01069	4.08779	0.01199	1.75037	0.00400	0.23739	−0.38187
	Exact[b]	2.5261	—	4.0873	—	1.7503	—	0.2383	—

[a] $W_{c'} = w_{c'}/(10^{-3}\times ql_c^4/D)$; $\bar{M}_{rc'} = M_{rc'}/(10^{-2}\times ql_c^2)$; $\bar{M}_{\theta c'} = M_{\theta c'}/(10^{-2}\times ql_c^2)$; $\bar{Q}_{\theta b'} = Q_{\theta b'}/ql_c$.
[b] Exact solution (Kobayshi and Turvey, 1994).

In Table 5, the effect of the inner to outer radii ratio, b/a, on the convergence rate of the DQEM results is examined. Since no analytical solutions have been found available for cases $b/a = 0.10$ and 0.25 in the open literature, the converged DQEM results obtained using 15×15 grid points in each element are used as the 'accurate solution' to define the relative error for these two cases in this table. It is evident that the convergence rate of the DQEM results increases only slightly as the inner to outer radii ratio, b/a, increases from 0.1–0.5. For all the cases analyzed here, however, a reasonably accurate numerical solution can be achieved with 11×11 grid points in each element.

4. Numerical application examples

The DQEM is now applied to analyze several Reissner–Mindlin plate bending problems described by the polar coordinates. The main purpose of this Section is to illustrate the applicability and flexibility of the DQEM developed in this paper for solving various kinds of static problems of Reissner–Mindlin plates. To ensure the accuracy of the numerical results, the grid points in

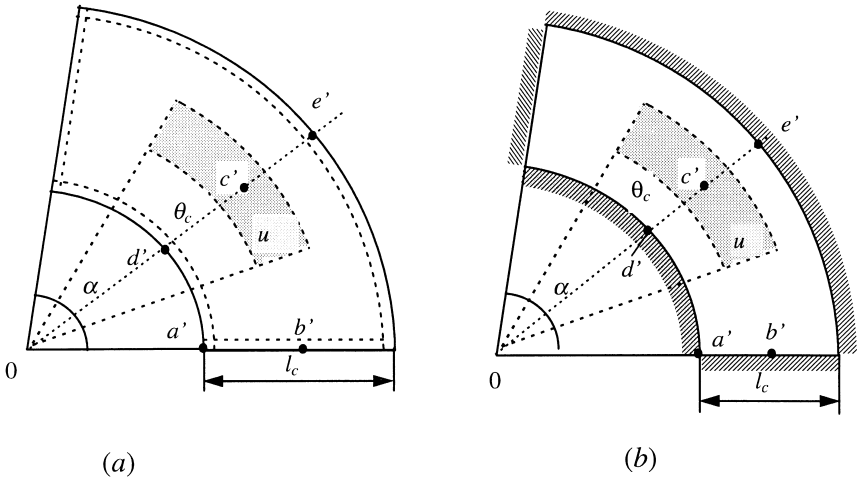

Fig. 7. Annual sector plates subjected to a patch load on the shadowed area with different constraint conditions: (a) a simply supported plate; (b) a fully clamped plate.

each element are set to 11×11 for the thick plates and 13×13 for the thin plates ($h/l_c = 0.01$). Poisson's ratio for all cases is taken to be 0.3.

4.1. Annular sector plate subjected to a patch load

The first application example analyzed here is the annular sector plate subjected to a uniformly distributed patch load over a sectorial area. Two boundary conditions (SSSS and CCCC) are considered as shown in Figs 7(a) and (b). The numerical results are presented in Tables 6 and 7. To verify the present results, some FEM solutions obtained using the commercial software package ANSYS (Version 5.3) are also tabulated. These FEM solutions are computed using a uniform mesh with 1825 grid points (active degree-of-freedom is 10,564). An eight-node shell 93 element was used. It is evident from Tables 6 and 7 that the present DQEM results are in excellent agreement with the FEM solutions. Moreover, it is observed that the sector angle α and the dimensions of the loading area, u/l_c and θ_c/α, have significant influences on the values of the deflection, moments and shear forces at the given points of the plates listed in these two tables. All the numerical results except $\bar{Q}_{\theta b'}$, increase with either the sector angle α or the dimensions of the loading area, u/l_c and θ_c/α. The values of $\bar{Q}_{\theta b'}$ in both Tables, on the other hand, decrease as the sector angle increases, but increase with the dimensions of the loading area. Furthermore, the data in both tables indicate that the increase in relative thickness leads to the increase of the normalized central deflection $W_{c'}$, but with very slight influence on the normalized moments and shear forces.

4.2. Annular sector plate with mixed boundary conditions

In order to demonstrate the applicability of the DQEM to bending analysis of plates with mixed boundary conditions in polar coordinates, an annular sector plate with simply supported circular peripheries and mixed radial boundary conditions (partially clamped and partially simply sup-

Table 6
Deflections, bending and twisting moments and shear forces of a simply supported annular sector plate subjected to a uniformly distributed patch load over a sectorial area (Fig. 7(a), $b/a = 0.5$)[a]

α	h/l_c	u/l_c	θ_c/α	$W_{c'}$	$\bar{M}_{rc'}$	$\bar{M}_{\theta c'}$	$\bar{M}_{r\theta a'}$	$\bar{Q}_{rd'}$	$\bar{Q}_{re'}$	$\bar{Q}_{\theta b'}$
30°	0.01	0.2	0.2	0.25361	0.61056	0.69895	−0.22618	0.01277	−0.01041	0.01823
		0.5	0.5	1.23602	2.01150	2.47776	−1.25829	0.07932	−0.06915	0.10478
	FEM[b]	0.5	0.5	1.23610	2.01817	2.28583	—	—	—	—
		0.8	0.8	2.13743	2.96054	3.80680	−2.52230	0.19892	−0.17975	0.22613
	0.2	0.2	0.2	0.36845	0.61063	0.69928	−0.23202	0.01185	−0.01051	0.01825
		0.5	0.5	1.62948	2.01168	2.47860	−1.29001	0.07478	−0.06992	0.10481
		0.8	0.8	2.73035	2.96097	3.80838	−2.58178	0.19034	−0.18125	0.22626
60°	0.01	0.2	0.2	0.89767	1.41628	1.08914	−0.45647	0.03885	−0.02588	0.01093
		0.5	0.5	4.29624	5.05340	3.31964	−2.59784	0.21098	−0.13863	0.07536
	FEM[b]	0.5	0.5	4.29634	5.07000	3.33017	—	—	—	—
		0.8	0.8	7.32760	7.78999	4.62861	−5.31998	0.42110	−0.28425	0.22051
	0.2	0.2	0.2	1.11981	1.41628	1.09113	−0.47522	0.03757	−0.02608	0.01077
		0.5	0.5	5.04283	5.05089	3.33031	−2.69954	0.20507	−0.13939	0.07548
		0.8	0.8	8.43947	7.78512	4.64887	−5.51087	0.41256	−0.28517	0.22083
90°	0.01	0.2	0.2	1.39893	1.98800	1.29455	−0.33857	0.05815	−0.03730	0.00546
		0.5	0.5	6.23309	6.77263	3.34071	−2.23852	0.27750	−0.16950	0.04257
	FEM[b]	0.5	0.5	6.22015	6.78500	3.35100	—	—	—	—
		0.8	0.8	10.1207	10.0757	4.21410	−5.47778	0.50047	−0.31728	0.17688
	0.2	0.2	0.2	1.69232	1.98840	1.29751	−0.35557	0.05654	−0.03754	0.00479
		0.5	0.5	7.14816	6.77055	3.35671	−2.34118	0.27281	−0.17013	0.04272
		0.8	0.8	11.4255	10.0727	4.24280	−5.69477	0.49592	−0.31760	0.17722

[a] $W_{c'} = w_{c'}/(10^{-3} \times ql_c^4/D)$; $\bar{M}_{rc'} = M_{rc'}/(10^{-2} \times ql_c^2)$; $\bar{M}_{\theta c'} = M_{\theta c'}/(10^{-2} \times ql_c^2)$; $\bar{M}_{r\theta a'} = M_{r\theta a'}/(10^{-2} \times ql_c^2)$; $\bar{Q}_{rd'} = Q_{rd'}/ql_c$; $\bar{Q}_{re'} = Q_{re'}/ql_c$; $\bar{Q}_{\theta b'} = Q_{\theta b'}/ql_{c'}$.

[b] The finite element results computed using the commercial software package ANSYS (Version 5.3) where shell 93 element was selected with 1825 grid points (actual number of active DOF: 10,564).

ported), as shown in Fig. 8, is considered. The plate is subjected to a uniformly distributed load over the entire plate. The results of the plate with an inner to outer radii ratio $b/a = 0.5$ for different sector angles and relative thicknesses are presented in Table 8. The converged results to three significant figures using the finite element software package ANSYS (Version 5.3) are also tabulated in the same table. These results are computed using an eight-node shell 93 element with a uniform mesh of 4033 grid points (active degree-of-freedom is 23,314). It is observed that the present DQEM solution agrees very well with the FEM results. This reveals that we can apply the DQEM confidently to the solution of polar plates with mixed boundary conditions.

4.3. A fully clamped annular sector plate with a free sectorial cutout

As shown in Fig. 9, a fully clamped and uniformly loaded annular sector plate with a sectorial free cutout is analyzed. The results of the deflections at three selected points, a', b', c' and the

Table 7
Deflections, bending moments and shear forces of a fully clamped annular sector plate subjected to a uniformly distributed patch load over a sectorial area (Fig. 7(b), $b/a = 0.5$)[a]

α	h/l_c	u/l_c	θ_c/α	$W_{c'}$	$\bar{M}_{rc'}$	$\bar{M}_{\theta c'}$	$\bar{Q}_{rd'}$	$\bar{Q}_{re'}$	$\bar{Q}_{\theta b'}$
30°	0.01	0.2	0.2	0.11366	0.44937	0.51822	0.01950	−0.01702	0.03343
		0.5	0.5	0.47336	1.15448	1.48451	0.12033	−0.10745	0.16771
	FEM[b]	0.5	0.5	0.47326	1.16030	1.49248	—	—	—
		0.8	0.8	0.68047	1.38121	1.88991	0.27828	−0.24297	0.30603
	0.2	0.2	0.2	0.23404	0.46936	0.51618	0.01007	−0.01279	0.02431
		0.5	0.5	0.89419	1.24642	1.47829	0.06698	−0.08481	0.13232
	FEM[b]	0.5	0.5	0.89418	1.25273	1.48627	—	—	—
		0.8	0.8	1.31599	1.50964	1.88930	0.18024	−0.21075	0.26442
60°	0.1	0.2	0.2	0.38971	1.02301	0.78751	0.07270	−0.04492	0.01362
		0.5	0.5	1.56833	2.91010	1.78885	0.33285	−0.20000	0.10383
	FEM[b]	0.5	0.5	1.56817	2.92600	1.79700	—	—	—
		0.8	0.8	2.2106	3.69554	1.97819	0.55078	−0.35163	0.29780
	0.2	0.2	0.2	0.62879	1.01848	0.82553	0.05070	−0.03836	0.00985
		0.5	0.5	2.39221	2.89583	1.94921	0.25756	−0.18687	0.00790
	FEM[b]	0.5	0.5	2.39223	2.91153	1.95833	—	—	—
		0.8	0.8	3.43031	3.69228	2.17645	0.47114	−0.34296	0.24283
90°	0.01	0.2	0.2	0.55813	1.34477	0.87541	0.10047	−0.06057	0.00202
		0.5	0.5	1.95880	3.43880	1.50543	0.35944	−0.21345	0.03857
	FEM[b]	0.5	0.5	1.95897	3.45800	1.50927	—	—	—
		0.8	0.8	2.56970	4.11462	1.45818	0.5374	−0.35333	0.22746
	0.2	0.2	0.2	0.87941	1.34213	0.92967	0.07531	−0.05391	0.00073
		0.5	0.5	2.97451	3.44531	1.66583	0.32252	−0.21156	0.02689
	FEM[b]	0.5	0.5	2.97451	3.46400	1.67067	—	—	—
		0.8	0.8	3.97362	4.13401	1.59005	0.52354	−0.35519	0.17980

[a] $W_{c'} = w_{c'}/(10^{-3} \times ql_c^4/D)$; $\bar{M}_{rc'} = M_{rc'}/(10^{-2} \times ql_c^2)$; $\bar{M}_{\theta c'} = M_{\theta c'}/(10^{-2} \times ql_c^2)$; $\bar{Q}_{rd'} = Q_{rd'}/ql_c$; $\bar{Q}_{re'} = Q_{re'}/ql_c$; $\bar{Q}_{\theta b'} = Q_{\theta b'}/ql_{c'}$.

[b] The finite element results computed using the commercial software package ANSYS (Version 5.3) where shell 93 element was selected with 1825 grid points (actual number of active DOF: 10,564).

moments and shear forces at the other three points, d', e', f', are computed and displayed in Table 9. Three sector angles, $\alpha = 30$, 60 and 90°, are considered. The computations were carried out for both thin ($h/l_c = 0.01$) and thick ($h/l_c = 0.2$) plates. The DQEM results are compared with those obtained using the finite element software package ANSYS (Version 5.3). Again, the shell 93 element with an even mesh (total grid points used: 2824; active DOF: 15,408) was chosen for computations. The comparison shows that both solutions are in good agreement.

5. Conclusion

In this paper, the two-dimensional differential quadrature element method has been developed for the bending analysis of Reissner–Mindlin plates in the polar coordinate system by integrating

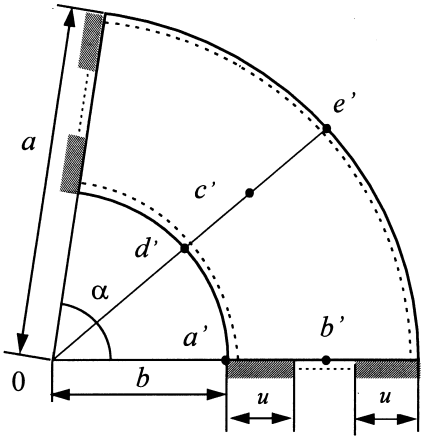

Fig. 8. A uniformly loaded annular sector plate having simply supported circular edges and mixed boundary conditions (CSC) on the radial edges.

Table 8
Deflections, bending moments and shear forces of a uniformly loaded annular sector plate with mixed boundary conditions (Fig. 8, $b/a = 0.5; u/l_c = 1/3; N_E = 3 \times 1$)[a]

α	h/l_c	Solutions	$W_{c'}$	$\bar{M}_{rc'}$	$\bar{M}_{\theta c'}$	$\bar{M}_{r\theta c}$	$\bar{Q}_{rd'}$	$\bar{Q}_{re'}$
30°	0.01	DQEM	1.24083	1.98726	2.64323	0.00000	0.15477	−0.21844
		FEM[b]	1.21562	1.94933	2.62133	0.00000	—	—
	0.20	DQEM	2.16730	2.33028	3.02051	0.00000	0.18575	−0.23398
		FEM[b]	2.14945	2.30180	2.98873	0.00000	—	—
60°	0.01	DQEM	6.22027	6.80788	4.57863	0.00000	0.45347	−0.35836
		FEM[b]	6.14121	6.70567	4.55967	0.04039	—	—
	0.20	DQEM	7.90020	7.30139	4.56674	0.00000	0.46312	−0.36330
		FEM[b]	7.85817	7.52600	4.58847	0.00006	—	—
90°	0.01	DQEM	10.0525	10.0758	4.46367	0.00000	0.59997	−0.41124
		FEM[b]	9.99020	9.98250	4.47083	0.00000	—	—
	0.20	DQEM	11.6782	10.2676	4.40273	0.00000	0.59297	−0.41029
		FEM[b]	11.6459	10.2307	4.43353	0.00000	—	—

[a] $W_{c'} = w_{c'}/(10^{-3} \times ql_c^4/D)$; $\bar{M}_{rc'} = M_{rc'}/(10^{-2} \times ql_c^2)$; $\bar{M}_{\theta c'} = M_{\theta c'}/(10^{-2} \times ql_c^2)$; $\bar{M}_{r\theta c} = M_{r\theta c'}/(10^{-2} \times ql_c^2)$; $\bar{Q}_{rd'} = Q_{rd'}/ql_c$; $\bar{Q}_{re'} = Q_{re'}/ql_c$.

[b] The finite element results computed using the commercial software package ANSYS (Version 5.3) where shell 93 element was selected with 4033 grid points (actual number of active DOF: 23,314).

the domain decomposition method with the DQ method. The detailed formulations for the sectorial DQEM Reissner–Mindlin plate bending element, and the compatibility conditions between adjacent elements have been derived in polar coordinates.

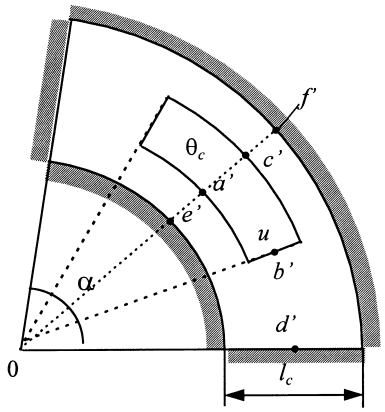

Fig. 9. A fully clamped and uniformly loaded annular sector plate with an inner free sectorial cutout.

Table 9
Deflections, bending moments and shear forces of a fully clamped and uniformly loaded annular sector plate having a sectorial cutout (Fig. 9, $u/l_c = \theta_c/\alpha = 0.5; b/a = 0.5; v = 0.3; N_E = 3\times 3$)[a]

α	h/l_c	$W_{a'}$	$W_{b'}$	$W_{c'}$	$\bar{M}_{re'}$	$\bar{M}_{rf}$	$\bar{M}_{0d'}$	$\bar{Q}_{re'}$	$\bar{Q}_{rf}$
30°	0.01	0.22224	0.19743	0.32810	−1.94329	−2.36111	−2.08510	0.27158	−0.26638
	FEM[b]	0.22195	0.19707	0.33222	−2.20333	−2.37700	−2.04950	—	—
	0.20	0.52835	0.42540	0.67198	−1.78844	−2.24862	−1.91542	0.21054	−0.22519
	FEM[b]	0.52593	0.42750	0.68916	−1.73873	−2.38073	−1.98107	—	—
60°	0.01	0.62075	1.10709	0.53013	−4.13854	−3.15798	−4.38428	0.31535	−0.24757
	FEM[b]	0.62029	1.10487	0.52549	−4.18833	−3.07317	−4.39583	—	—
	0.20	1.03988	1.92673	0.87173	−3.97269	−3.11610	−3.86942	0.31342	−0.24309
	FEM[b]	1.03584	1.92395	0.84945	−4.00393	−3.05280	−3.87607	—	—
90°	0.01	0.62257	1.82579	0.50870	−3.99062	−3.03478	−5.29256	0.26819	−0.23920
	0.20	1.02633	3.10989	0.83393	−4.10449	−3.00865	−4.35417	0.30017	−0.23480

[a] $W_{a'} = w_{a'}/(10^{-3}\times ql_c^4/D)$; $W_{b'} = w_{b'}/(10^{-3}\times ql_c^4/D)$; $W_{c'} = w_{c'}/(10^{-3}\times ql_c^4/D)$; $\bar{M}_{re'} = M_{re'}/(10^{-2}\times ql_c^2)$; $\bar{M}_{0d'} = M_{0d'}/(10^{-2}\times ql_c^2)$; $\bar{M}_{rf} = M_{rf'}/(10^{-2}\times ql_c^2)$; $\bar{Q}_{re'} = Q_{re'}/ql_c$; $\bar{Q}_{rf} = Q_{rf'}/ql_c$.

[b] The finite element results computed using the commercial software package ANSYS (Version 5.3) where shell 93 element was selected with 2824 grid points (actual number of active DOF: 15,408)

The convergence properties and accuracy of the DQEM for solving the bending of the Reissner–Mindlin polar plates have been investigated through a number of numerical studies. It was found that the convergence rate of the DQEM in the polar coordinate system is dependent mainly upon the boundary conditions and plate relative thickness. The effects of the sector angle and inner to outer radii ratio on the convergence rate are not significant. However, for all the cases analyzed

here, an accurate solution was achieved with 11×11 grid points in each element for a thicker plate ($h/l_c \geqslant 0.1$) and 13×13 grid points in each element for a thin plate ($h/l_c = 0.01$).

Consequently, this new method has been successfully applied to the analysis of several annular sector plates with discontinuities in loading, geometry and boundary conditions. The validity of the DQEM has been further established by comparing the DQEM results for these example plate problems with the FE solutions obtained using the commercial FEM software ANSYS (Version 5.3). It is found that the DQEM integrates both the advantages of DQM and the flexibility of the FEM for thick polar plate analysis and therefore, has greatly enhanced the application scopes of the DQM.

References

Bellman, R.E., Casti, J., 1971. Differential quadrature and long term integration. J. Math. Analysis Appl. 34, 235–238.

Bellman, R.E., Kashef, B.G., Casti, J., 1972. Differential quadrature: a technique for the rapid solution on non-linear partial differential equations. J. Computa. Phys. 10, 40–52.

Bert, C.W., Jang, S.K., Striz, A.G., 1988. Two new approximate methods for analyzing free vibration of structural components. AIAA J. 26, 612–618.

Bert, C.W., Jang, S.K., Striz, A.G., 1989. Nonlinear bending analysis of orthotropic rectangular plates by the method of differential quadrature. Computa. Mech. 5, 217–226.

Bert, C.W., Malik, M., 1995. Differential quadrature analysis of free vibration of symmetric cross-ply laminates with shear deformation and rotatory inertia. Shock and Vibr. 2, 321–338.

Bert, C.W., Malik, M., 1996a. Differential quadrature method in computational mechanics: a review. Appl. Mech. Rev. 49, 1–28.

Bert, C.W., Malik, M., 1996b. The differential quadrature method for irregular domains and application to plate vibration. Int. J. Mech. Sci. 38, 589–606.

Bert, C.W., Malik, M., 1996c. Semianalytical differential quadrature solution for free vibration analysis of rectangular plates. AIAA J. 34, 601–606.

Chen, W., Striz, A.G., Bert, C.W., 1997a. Free vibration of high-accuracy plate elements by the quadrature element method. J. Sound Vibr. 202, 689–702.

Chen, W., Striz, A.G., Bert, C.W., 1997b. A new approach to the differential quadrature method for fourth-order equations. Int. J. Numer. Methods Engrg 40, 1941–1956.

Civan, F., Sliepcevich, C.M., 1984. Differential quadrature for multidimensional problems. J. Math. Analysis Appl. 101, 423–443.

Han, J.-B., Liew, K.M., 1996. The differential quadrature element method (DQEM) for axisymmetric bending of thick circular plates. Proc. of the Third Asian–Pacific Conf. on Comput. Mechanics, pp. 2363–2368.

Kobayashi, H., Sonoda, K., 1987. Mindlin's plate equations in polar coordinates for elastic foundation problems. Mem. Fac. Eng., vol. 28. Osaka City University, pp. 187–195.

Kobayashi, H., Turvey, G.J., 1994. Elastic small deflection analysis of annular sector Mindlin plates. Int. J. Mech. Sci. 36 (9), 811–827.

Liew, K.M., Han, J.-B., Xiao, Z.M., Du, H., 1996. Differential quadrature method for Mindlin plates on Winkler foundations. Int. J. Mech. Sci. 38, 405–421.

Liu, F.-L., Liew, K.M., 1998. Static analysis of Reissner–Mindlin plates by differential quadrature element method. Trans. ASME, J. Appl. Mech. 65, in press.

Malik, M., Bert, C.W., 1996. Implementing multiple boundary conditions in the DQ solution of higher order PDE's: application to free vibration of plates. Int. J. Numer. Meth. Engrg 39, 1237–1258.

Mindlin, R.D., 1951. Influence of rotatory inertia and shear on flexural motion of isotropic, elastic plates. Trans. ASME, J. Appl. Mech. 18, 31–38.

Pandya, M.D., Sherbourne, A.N., 1991. Buckling of anisotropic composite plates under stress gradient. ASCE J. Engrg Mechanics 117, 260–275.

Reissner, E., 1945. The effect of transverse shear deformation on the bending of elastic plates. Trans. ASME J. Appl. Mech. 12, 69–77.

Reissner, E., 1947. On bending of elastic plates. Quart. Appl. Math. 5, 55–68.

Striz, A.G., Chen, W., Bert, C.W., 1994. Static analysis of structures by the quadrature element method (QEM). Int. J. Solids Struct. 31, 2807–2818.

Striz, A.G., Jang, S.K., Bert, C.W., 1988. Non-linear bending analysis of thin circular plates by differential quadrature. Thin-Walled Struct. 69, 51–62.